Zou *et al. Journal of Nanobiotechnology* (2025) 23:126
https://doi.org/10.1186/s12951-025-03182-8

Journal of Nanobiotechnology

RESEARCH Open Access

Targeting GDF15 to enhance immunotherapy efficacy in glioblastoma through tumor microenvironment-responsive CRISPR-Cas9 nanoparticles

Cheng Zou[1†], Xiao Liu[2†], Weizhong Wang[2†], Lei He[1], Anan Yin[3,4], Zhengcong Cao[1], Maorong Zhu[1], Yuxin Wu[1], Xiaolin Liu[1], Jiying Ma[1], Yalong He[2], Shuning Wang[1], Wangqian Zhang[1], Wei Liu[2], Yingqi Zhang[1], Jintao Gu[1*], Wei Lin[2,5*], Kuo Zhang[1*] and Meng Li[1*]

Abstract

Despite the outstanding clinical success of immunotherapy, its therapeutic efficacy in glioblastoma (GBM) is still limited. To identify critical regulators of GBM immunity, we constructed a mouse single-guide RNA (sgRNA) library corresponding to all disease-related immune genes, and performed an in vivo CRISPR knockout (KO) screen in syngeneic GBM mouse models. We demonstrated that the deletion of GDF15 in GBM cells ameliorated the immunosuppressive tumor microenvironment (TME) and enhanced the antitumor efficacy of immune checkpoint blockade (ICB) response. Moreover, we designed unique nanoparticles for efficient encapsulation of CRISPR-Cas9, noninvasive brain delivery and tumor cell targeting, demonstrating an effective and safe strategy for GDF15 gene therapy. The CRISPR-Cas9 nanoparticles, known as ANP_{SS} (Cas9/sgRNA), are easily created by enclosing a single Cas9/sgRNA complex in a polymer shell that is sensitive to glutathione. This shell also contains a dual-action ligand that aids in crossing the blood–brain barrier, targeting tumor cells, and selectively releasing Cas9/sgRNA. Our encapsulating nanoparticles demonstrated promising GBM targeting, resulting in high GDF15 gene editing efficiency within brain tumors while showing minimal off-target gene editing in high-risk tissues. Treatment with ANP_{SS} (Cas9/sgGDF15) effectively halted tumor growth, reversed immune suppression, and enhanced the efficacy of ICB therapy. These results emphasize the potential role of GDF15 in modulating the immune microenvironment and enhancing the effectiveness of current immunotherapy strategies for GBM.

†Cheng Zou, Xiao Liu and Weizhong Wang contributed equally to this work

*Correspondence:
Jintao Gu
gujintao@fmmu.edu.cn
Wei Lin
linwei@fmmu.edu.cn
Kuo Zhang
justy1985@126.com
Meng Li
limeng@fmmu.edu.cn

Full list of author information is available at the end of the article

Key points

1. In vivo CRISPR screens identify GDF15 as a critical driver of immune escape.
2. Synthesis of TME-responsive nanoparticles for GDF15 gene editing therapy.
3. GDF15 gene editing therapy enhances the antitumor efficacy of immune checkpoint blockade (ICB) response.

Graphical Abstract

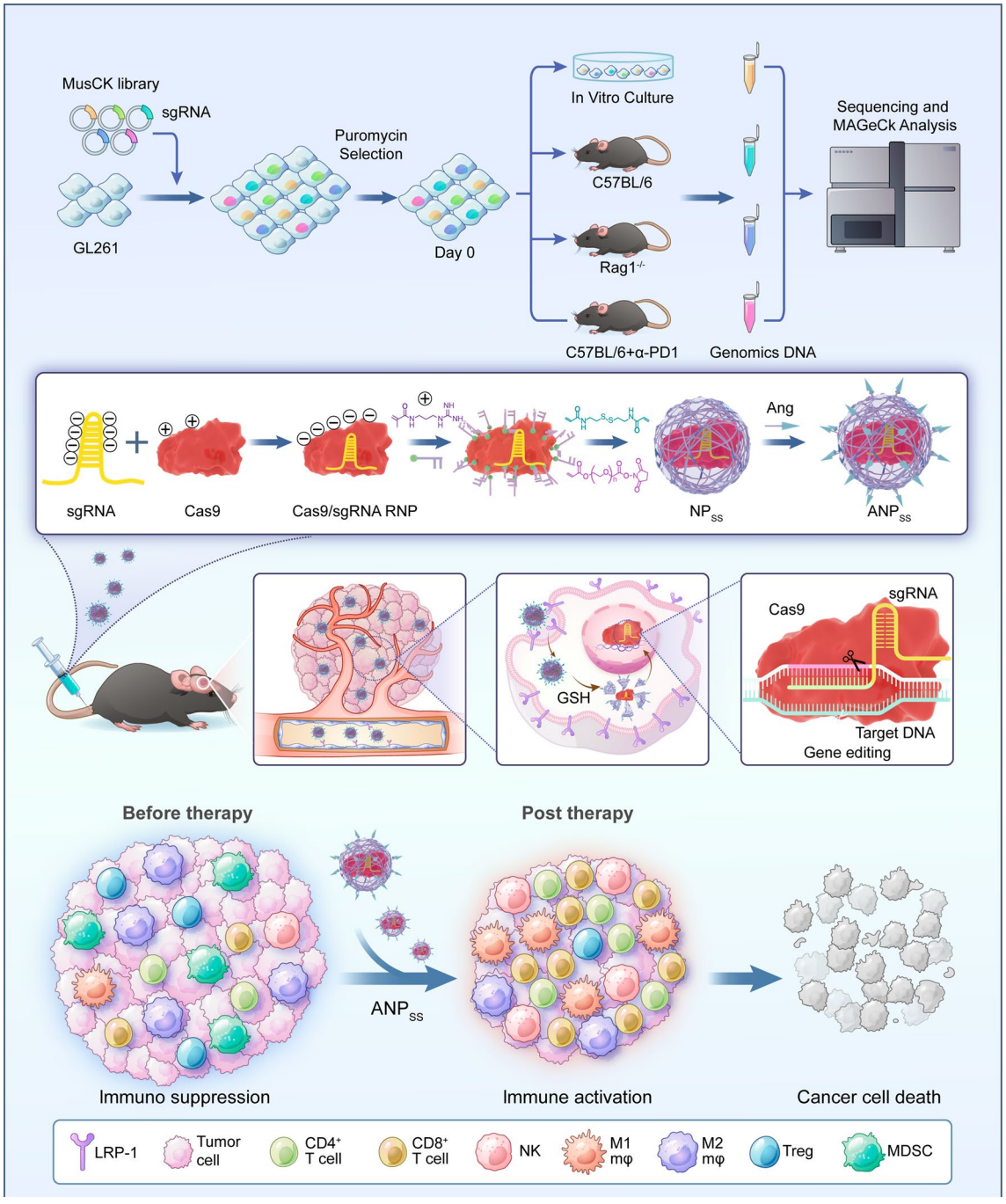

Introduction

Glioma is the most common primary brain tumor, and glioblastoma (GBM), the most aggressive subtype, accounts for approximately half of glioma cases [1]. Standard treatments, such as surgical intervention, radiotherapy, pharmacotherapy (often using temozolomide as a chemotherapeutic agent), and tumor-treating fields (TTFields), have yielded only modest advancements in increasing the survival rates of GBM patients [2]. The lack of progress in GBM treatment can be attributed to various factors, such as invasive tumor growth in critical organs hindering local therapy, the shielding of tumor cells by the blood–brain barrier (BBB), cancer cell resistance to cell death induction and the lack of targeted pharmacological agents [3, 4]. Additionally, the distinct immune microenvironment of the central nervous system must be taken into account when exploring immune-based treatments for GBM [5].

Immunotherapy has been widely proven as an effective treatment for different types of solid tumors, such as hepatocellular carcinoma, stomach cancer, lung cancer, and colon cancer [6]. This progress represents a great development in the increasingly important field of immunotherapy, which is centered around the idea of utilizing the patient's own immune system to combat cancerous growth. Current immunotherapy approaches for cancer treatment focus mainly on the use of immune checkpoint blockade (ICB) agents [7]. Additionally, therapeutic vaccines, CAR-T, and oncolytic viruses are also key elements in present immunotherapeutic strategies [8]. Patients with GBM enrolled in clinical trials are currently experiencing limited benefits from immunotherapeutic approaches, largely attributed to the 'cold' immune microenvironment within GBM tumors [9]. The challenges arise from the absence of universally applicable tumor-specific antigen targets and the presence of an immune-suppressive microenvironment that hinders T-cell penetration and activation within the tumor [10]. Therefore, there is an urgent need for the development of innovative therapeutic approaches to combat protumor immune responses and address the resistance of tumors to immunotherapy within the microenvironment, specifically for the treatment of GBM.

Numerous studies have been conducted to investigate the components and interactions between immune cells and tumor cells in the tumor microenvironment (TME). Moreover, CRISPR screens have significantly improved genome editing, enabling the identification of previously unknown genes linked to immunotherapy responses. Multiple tumor-intrinsic modulators of programmed death ligand 1 (PD-L1) or MHC-I have been identified through flow cytometry-based in vitro screens [11, 12]. These modulators may play a role in tumor cell immune escape from killing by cytotoxic T lymphocytes. Utilizing subcutaneous tumor models established with a variety of cancer cell lines from different sources, combined in vivo screening revealed a fundamental group of shared genes, including Ptpn2, Setdb1, Pbrm1 and Cop1, whose absence could increase the effectiveness of ICB immunotherapy [13–16]. Owing to the diverse nature of the TME in various syngeneic tumor models, these in vitro screens and subcutaneous tumor models may not accurately reflect the intricate interactions between tumors and the immune system within the TME of tumors that arise naturally. Orthotopic tumor models are considered a more relevant tool for screening antitumor immunity targets, although they present technical challenges and may not be feasible for genome-wide screening. Due to the complexity of the immune system, it is advisable to apply multiple immune selective pressures to identify clinically relevant targets using high-throughput in vivo CRISPR screens. Nevertheless, a targeted functional genetic screen utilizing an orthotopic GBM model has not yet been employed to systematically identify biologically relevant immune targets.

Here, we performed in vivo CRISPR screens targeting disease-related immune genes under different immune selective pressures. By comparing the glioma cohort data and functional screening results, we pinpointed growth differentiation factor-15 (GDF15) as a key factor in immune evasion and a potential target to sensitize patients to ICB immunotherapy. Mechanistic and functional investigations demonstrated that GDF15 ablation remodeled the TME, ameliorating the immunosuppressive microenvironment. Compared with the current immunotherapies used to antitumor immunity, directly suppressing GDF15 expression in tumor cells through genome editing offers distinct advantages, including high specificity and long-term therapeutic effects. To achieve this goal, we loaded Cas9 ribonucleoprotein (RNP), complexed with single guide RNA (sgRNA), into angiopep-2-decorated, glutathione (GSH)-responsive nanoparticles [ANP_{SS}(Cas9/sgGDF15)] to construct a noninvasive brain delivery system. Treatment with ANP_{SS}(Cas9/sgGDF15) significantly suppressed tumor growth and altered the immune microenvironment in various GBM models. Furthermore, editing gene that target GDF15 has the potential to increase the efficacy of PD1 monoclonal antibody therapy, resulting in either complete or partial tumor regression and extended survival. The integration of CRISPR screens and CRISPRCas9 gene therapy represents a powerful approach for identifying and regulating potential therapeutic targets in various tumors.

Results

In vivo CRISPR screens identify GDF15 as a critical driver of immune escape

To systematically identify gene targets whose loss enhances antitumor immunity, we used a murine lentiviral CRISPR-Cas9 knockout (MusCK) library. This library includes 5 sgRNAs for each of the more than 4,900 genes implicated in tumor immune modulation. Once we validated the MusCK library, our subsequent step was to transduce the lentiviral MusCK library into Luc-expressing GL261 cells. Following in vitro passage to enable gene editing, we proceeded to transplant the tumor cells into designated regions of the brains of mice to establish orthotopic GBM models. The mouse types used for the orthotopic GBM models included: C57BL/6 mice, immunodeficient Rag1$^{-/-}$ mice—lacking both T cells and B cells and C57BL/6J mice subjected to PD-1 blockade treatment with a monoclonal antibody. (Fig. 1A). These treatments were used to generate an adaptive immune response strong enough to exert immune selective pressure on tumor cells. After 14 days, the mice were euthanized, and the tumors were harvested for high-throughput sgRNA library sequencing, after which significantly different levels of tumor growth were observed among the different model mice. T-cell-deficient Rag1$^{-/-}$ mice had the largest tumors, and immune-competent mice treated with an anti-PD-1 antibody had the smallest tumors (Fig. 1B). While the library representation of primary lentiviral and pretransplanted tumor cells (day 0) followed a log-normal distribution, the library representation of posttransplanted cells obtained from tumor masses from C57BL/6 and Rag1$^{-/-}$ mice showed a distinct shift (Fig. 1C).

Next, the CRISPR/Cas9 knockout screening readout from the C57BL/6 group was compared to those of the α-PD-1 and Rag1$^{-/-}$ groups. The analysis revealed that three genes (GDF15, SIK2, and CPLX2) overlapped and were found to be associated with the immune response in glioma (Fig. 1D-E and Supplementary Fig. 1). We sought to further investigate crucial immune-related genes in the complex TME that are involved in antitumor activities as possible targets for immunotherapy in GBM. Next, validation of the three genes was conducted using The Cancer Genome Atlas (TCGA), the Chinese Glioma Genome Atlas (CGGA), and a Gene Expression Omnibus (GEO) dataset uploaded by Gravendeel, LA. Strikingly, the analysis of the datasets from all three public databases revealed a notable correlation between increased levels of GDF15 and unfavorable prognosis (Fig. 1F). Conversely, no discernible effect on patient prognosis was observed in relation to SIK2 and CPLX2 (Supplementary Fig. 2). Furthermore, we examined the correlations among the three genes and CD8$^+$ T cells using the Tumor Immune Estimation Resource (TIMER) database. The results revealed that only GDF15 is negatively correlated with infiltration of CD8$^+$ T cells (Supplementary Fig. 3). We primarily examined gliomas classified as World Health Organization (WHO) grades II, III, or IV from the TCGA, CGGA, and GEO datasets. The findings indicated a rise in GDF15 expression in high-grade glioma (Fig. 1G). Our clinical specimens further supported the finding that GDF15 expression was significantly higher in high-grade glioma compared to low-grade glioma (Supplementary Fig. 4). To investigate the potential association between GDF15 and prognosis in glioma patients, we performed immunohistochemistry (IHC) analysis of GDF15 expression on a human tissue microarray comprising 180 glioma tumors. Among the 180 samples, a rise in GDF15 levels was observed among glioma patients who later experienced relapse. The fraction of individuals displaying elevated GDF15 expression was notably decreased within the nonrelapsed patient cohort in contrast to the relapsed cohort upon segregating patients into high and low GDF15 expression categories (Fig. 1H). These data suggest a potential association between GDF15 and relapse in glioma patients. Meanwhile, elevated GDF15 expression was shown to significantly influence the outcomes of both nonrelapsed and relapsed glioma patients (Fig. 1I). These findings indicate a strong correlation between GDF15 overexpression in tumor cells, an immunosuppressive TME and unfavorable patient survival outcomes.

GDF15 ablation promotes M1-like macrophage polarization and T-cell activation

To further investigate the role of GDF15 in GBM, we individually knocked out GDF15 in GL261 cell lines using three sgRNAs obtained from the CRISPR-Cas9 knockout (MusCK) library (Supplementary Fig. 5). Surprisingly, our study revealed that GDF15 did not exhibit an intrinsic role in tumor proliferation and apoptosis in vitro (Supplementary Fig. 6A-C). Furthermore, we inoculated murine glioma cells into immunodeficient mice (Rag1$^{-/-}$), and no obvious differences were detected between the sgGDF15 group and the corresponding control (Fig. 2A). However, when GL261 cells were inoculated into the brains of normal syngeneic mice (C57BL/6), the knockout of GDF15 significantly suppressed tumor growth, extended the lifespan of the mice, and reduced GDF15 concentrations in both the circulation and tumor microenvironment back to a physiological level (Fig. 2B and Supplementary Fig. 7). Thus, GDF15 failed to impede tumor cell proliferation in immunodeficient mice but impaired tumor progression in immunocompetent mice, indicating that the anti-tumor effect mediated by GDF15 may rely on the TME. These results prompted further investigation into how GDF15 shapes the TME in vivo.

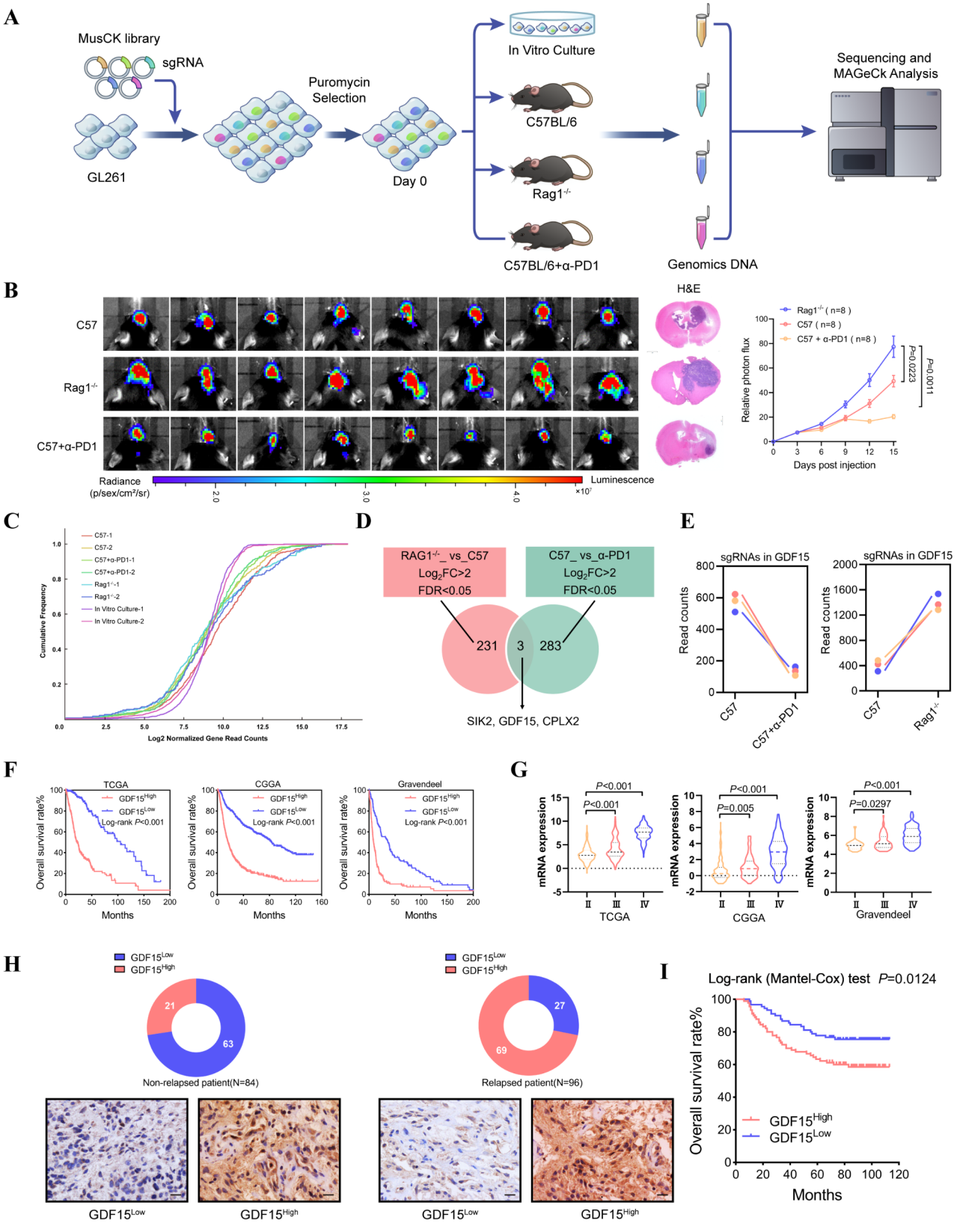

Fig. 1 (See legend on next page.)

(See figure on previous page.)

Fig. 1 In Vivo CRISPR screens identify GDF15 as a critical driver of immune evasion. **(A)** Workflow of in vivo CRISPR screens to identify potential therapeutic targets involved in GBM immune evasion. **(B)** Time course luminescence images of mice bearing orthotopic GL261-Luc tumors following different treatments ($n = 8$ mice in each group). **(C)** Cumulative distribution function plots of MusCK library sgRNAs in cells before transplantation, tumors in C57/B6 mice, and tumors in Rag1 mice and C57BL/6 mice subjected to PD-1 blockade treatment. **(D)** Venn diagram of the two criteria used to identify candidate gene hits. **(E)** Dynamic distribution of sgRNA read counts of enriched genes. **(F)** Prognostic value of GDF15 in the TCGA, CGGA, and Grvaendeel databases. **(G)** The expression level of GDF15 was correlated with the pathological stage of glioma in the TCGA, CGGA, and Gravendeel databases. **(H)** Representative images of IHC staining of GDF15 in samples from nonrelapsed and relapsed patients. **(I)** Kaplan–Meier estimate of survival time for glioma patients with low versus high expression of GDF15

We further used single-cell mass cytometry (CyTOF) to analyze immune cell infiltration in GDF15-deficient GL261 or control tumors derived from C57BL/6 mice. After being stained with 42 heavy metal-labeled antibodies, immune cells were categorized using a validated, data-driven, unsupervised clustering method (Fig. 2C). By employing the t-distributed stochastic neighbor embedding (tSNE) algorithm, $CD45^+$ immune cells were visually represented. The results of these assessments revealed that the $CD45^+$ cell population could be divided into 24 unique clusters (Fig. 2D-E). Further investigation was conducted on the variances within these clusters between the sgGDF15 and sgNC groups. The sgGDF15 group exhibited a marked increase in the numbers of $CD8^+$ effector T cells (cluster 4) and M1 macrophages (cluster 21). Conversely, the sgGDF15 group presented significant decreases in the numbers of $CD8^+$ exhausted T cells (cluster 9) and M2 macrophages (cluster 20) (Fig. 2F-G).

The expression of major immune cell markers in tumor-infiltrating immunocytes (TILs) was analyzed across different groups. The CyTOF results showed a notable increase in the proportion of $CD8^+CD69^+$ T cells after GDF15 knockout (Fig. 2H). CD69 expression is known to be rapidly upregulated upon activation in various leukocytes, making it a commonly used marker for activated T cells and NK cells [17]. Furthermore, the expression of T-cell exhaustion markers, such as PD1 and TIM3, was significantly reduced in the GDF15 knockout group. Moreover, analysis of the expression of markers associated with macrophages revealed that the levels of iNOS, CD86 and MHC II, which are markers of M1 macrophages, substantially increased following GDF15 knockout. In contrast, the expression levels of CD206 and CD163, which are markers of suppressive TAMs, decreased in the sgGDF15 group (Fig. 2H). The tumor tissues were stained for DAPI, PanCK, CD86, CD206, CD8, and GZMB using multiplex immunofluorescence. Our research indicated that tumors in the sgGDF15 group harbored a greater number of $CD8^+$ CTLs than sgNC group. Similarly, there was a notable reduction in the proportion of $CD206^+$ M2 macrophages within the tumor tissue (Fig. 2I). Moreover, the flow cytometry findings also indicated that, compared with the sgNC group, the sgGDF15 group presented the greatest quantity of $CD3^+CD8^+GZMB^+$ CTLs. Furthermore, the mice in the sgGDF15 group displayed low $CD86^-CD206^+$ TAM (M2-like TAM) infiltration into tumors and high $CD86^+CD206-$ TAM (M1-like TAM) infiltration within the tumors (Fig. 2J and Supplementary Fig. 8). These findings indicate that disrupting GDF15 has the potential to reshape the immunosuppressive TME by increasing M1-like infiltration and activating $CD8^+$ T cells.

Synthesis and characterization of TME-responsive nanoparticles for GDF15 gene editing therapy

Our above research indicated that GDF15 has the potential to alter the tumor immune microenvironment and facilitate GBM progression, identifying it as a key target for GBM immunotherapy. Compared with current immunotherapies such as adoptive immune cells or ICB, directly inhibiting the expression of GDF15 in tumor cells via genome editing offers superior advantages in the restoration of antitumor immunity. This includes enhanced specificity and prolonged therapeutic effects. However, the use of viral vectors to deliver the CRISPR-Cas9 system into organisms for effective editing of tumor sites is impeded by issues of specificity and biosecurity. To overcome this issue, we constructed nanoparticles cross-linked with a disulfide bond loaded with Cas9 and sgRNA targeting GDF15 [NP_{SS}(Cas9/sgGDF15)]. These nanoparticles were fabricated through an effective in situ polymerization technique employing free radicals. The Cas9/sgRNA complex was encapsulated with positively charged acrylate guanidine through electrostatic interactions, followed by polymerization and cross-linking with N, N'-bis(acryloyl) cystamine and polyethylene glycol (PEG) with acrylate- or succinate-decorated end-groups. Then the resulted nanoparticles were decorated with Angiopep-2 on their surface by an amidation reaction. (Fig. 3A). Angiopep-2 specifically binds to the low-density lipoprotein receptor (LRP-1), which is highly expressed on the surfaces of blood-brain barrier (BBB) endothelial cells and glioblastoma (GBM) tumor cells, thereby facilitating BBB penetration and the active targeting of tumor cells [18, 19]. Dynamic light scattering (DLS) was performed to determine the size of the nanoparticles, and the results revealed that the size and polydispersity index (PDI) of ANP_{SS}(Cas9/sgGDF15) were 124 nm and 0.12, respectively (Fig. 3B). The zeta potential of ANP_{SS}(Cas9/sgGDF15) was $\approx +24.65 \pm 3.79$ Mv (Fig. 3C). Moreover, we employed transmission electron microscopy (TEM)

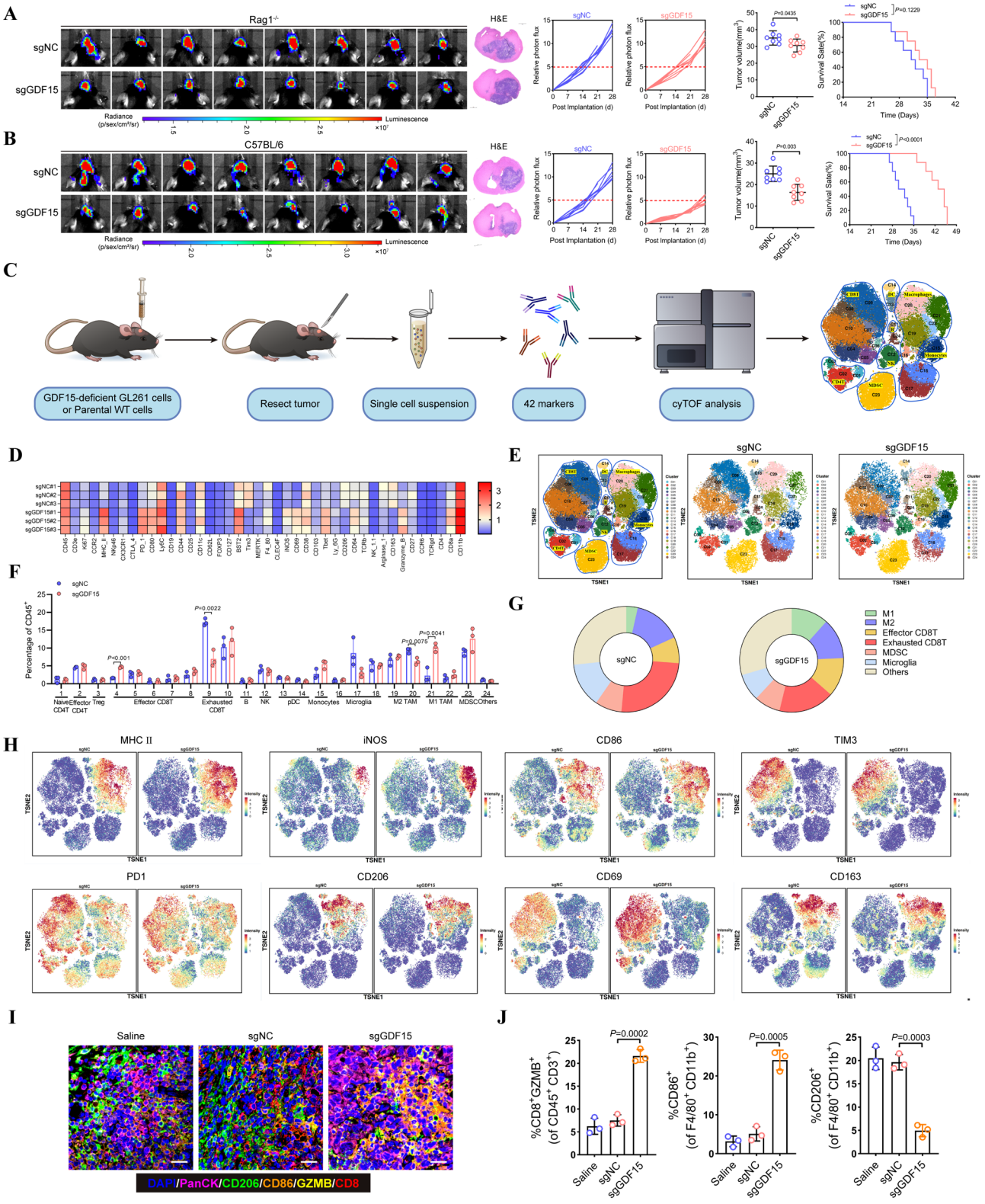

Fig. 2 (See legend on next page.)

(See figure on previous page.)

Fig. 2 GDF15 modulates the immune profile and impairs the antitumor T-cell response. **(A)** Luminescence images of mice bearing orthotopic GL261-Luc tumors in different groups ($n = 8$ mice in each group); Proliferation curves of tumors orthotopically transplanted into GL261-bearing Rag1$^{-/-}$ mice; Kaplan–Meier survival curves of GL261-bearing Rag1$^{-/-}$ mice. **(B)** Luminescence images of GL261 tumor-bearing C57BL/6 mice ($n = 8$ mice in each group); Proliferation curves of orthotopically transplanted tumors in GL261-bearing C57BL/6 mice; Kaplan–Meier survival curves of GL261-bearing C57BL/6 mice. **(C)** Schematic illustration of the CyTOF analysis of the immune response landscape in different groups. **(D)** Heatmap displaying the normalized expression of selected markers in each group. **(E)** t-SNE plots of immune cells in tumor tissues from each group. **(F)** The cell type corresponding to each cluster and the proportion of each cell type in the sgNC group and sgGDF15 group. **(G)** Relative abundance of tumor-infiltrating immune cell subpopulations based on CyTOF analysis. **(H)** tSNE visualization of CD206, iNOS, CD86, TIM3, CD69, PD1, MHC II, and CD163 expression. **(I)** Multiplex immunofluorescence analysis of PanCK, CD8, GZMB, CD86, and CD206 expression. Scale bar, 50 μm. **(J)** Flow cytometric quantification of CD206$^+$ TAMs, CD86$^+$ TAMs, and CD3$^+$CD8$^+$GZMB$^+$ T cells in tumors

to view the morphology of ANP_{SS}(Cas9/sgGDF15), validating their spherical structure. Notably, the nanoparticles exhibited rapid degradation and released Cas9/sgGDF15 in an intracellular reducing environment simulating high GSH levels. Interestingly, this phenomenon was not seen in the nonreducible control environment (Fig. 3D). Next, we investigated the potential of nanoparticle-mediated Cas9/sgGDF15 delivery for gene editing in vitro. We introduced the nanoparticles into GL261 cells, and the Cas9/sgRNA complex was used to identify target DNA sequences. Upon identifying a match, the Cas9 protein cleaved the DNA at the precise location, resulting in a double-stranded break (DSB) within the DNA. Subsequently, the cell activated its repair mechanism, primarily through nonhomologous end joining (NHEJ) (Fig. 3E). To evaluate the efficacy of our CRISPR/Cas9 nanoparticles in GDF15 gene editing and their ability to protect sgRNA, we performed T7 endonuclease I (T7E1) cleavage assays. Notably, the presence of RNase did not significantly affect the efficiency of ANP_{SS}(Cas9/sgGDF15)-mediated gene editing, which displayed an efficacy similar to that of free Cas9/sgGDF15 in an environment devoid of RNase. However, the introduction of RNase hindered the ability of free Cas9/sgGDF15 to cleave DNA (Fig. 3F). The efficiency and specificity of GDF15 gene disruption by ANP_{SS}(Cas9/sgGDF15) in GL261 cells were further evaluated through sanger sequencing. The results revealed that the editing site of the CRISPR/Cas9 system was located 3–5 bases ahead of the adjacent motif (PAM) sequence of the protospacer (Fig. 3G). Consistently, the ELISA results revealed that GDF15 protein secretion was reduced to 23.1% in the supernatant when treated with ANP_{SS}(Cas9/sgGDF15) nanoparticles, while ANP_{SS}(Cas9/sgNC) and saline did not cause a significant alteration in GDF15 secretion (Supplementary Fig. 9). These findings collectively show that ANP_{SS}(Cas9/sgGDF15) nanoparticles are capable of achieving precise GDF15 gene editing within GL261 cells. The disulfide cross-linking within the nanoparticles is essential for the specific release of Cas9/sgRNA, thus enhancing the safety of gene editing.

The escape of the nanoparticle content from endosomal confinement is necessary for its functionality, and we examined the endosomal escape capability of ANP_{SS}(Cas9/sgGDF15). ANP_{SS}(Cas9/sgGDF15) strongly colocalized with endosomes after 3 h of incubation. Moreover, ANP_{SS}(Cas9/sgGDF15) also highly colocalized with lysosomes after 3 h of incubation, suggesting their trafficking and accumulation to the lysosome. Interestingly, after 6 h of incubation, most of the ANP_{SS}(Cas9/sgGDF15) and endosomes/lysosomes did not overlap, suggesting that ANP_{SS}(Cas9/sgGDF15) escaped from endosomes/lysosomes over time (Supplementary Fig. 10A-B). Moreover, after long-term storage at room temperature and in medium containing 10% FBS, the ANP_{SS}(Cas9/sgGDF15) remained relatively constant in size, indicating satisfactory stability (Supplementary Fig. 11).

To assess the nanoparticles' ability to target GBM cells, we labeled the Cas9 protein with FITC and the sgRNA with sulfo-cyanine5.5 (Cy5.5) before encapsulating them in the nanoparticles. Subsequently, we developed an in vitro BBB model by culturing a monolayer of bEnd.3 cells. Confocal microscopy imaging demonstrated that ANP_{SS}(Cas9/sgGDF15) possessed the highest targeting efficiency compared with NP_{SS}(Cas9/sgGDF15) (Fig. 3H). We then investigate the biodistribution of the nanoparticles in vivo, fluorescence images were captured at various time points using an IVIS Spectrum system following the intravenous administration of ANP_{SS}(Cas9/sgGDF15) or NP_{SS}(Cas9/sgGDF15). Compared with that of NP_{SS}(Cas9/sgGDF15), the fluorescence intensity of ANP_{SS}(Cas9/sgGDF15) was greater in the brain (Fig. 3I, **upper panel**). Given that LDL receptor-related protein 1 (LRP1) is overexpressed by both endothelial cells of the BBB and GL261 glioma cells, LRP-1–targeting angiopep-2–functionalized ANP_{SS}(Cas9/sgGDF15) are expected to increase BBB permeability via receptor-mediated transcytosis. The fluorescent signal of Cy5.5 emitted by the ANP_{SS}(Cas9/sgGDF15) group appeared brighter than that of the NP_{SS}(Cas9/sgGDF15) group during ex vivo imaging of mouse brains (Fig. 3I, **lower panel**). More importantly, the predominant localization of ANP_{SS}(Cas9/sgGDF15) occurred within the confines of the tumor border, indicating its exceptional ability to target tumor cells (Fig. 3J). Considering that the microenvironment of a tumor produced by a cancer cell line varies from that of a tumor that arises naturally, we also

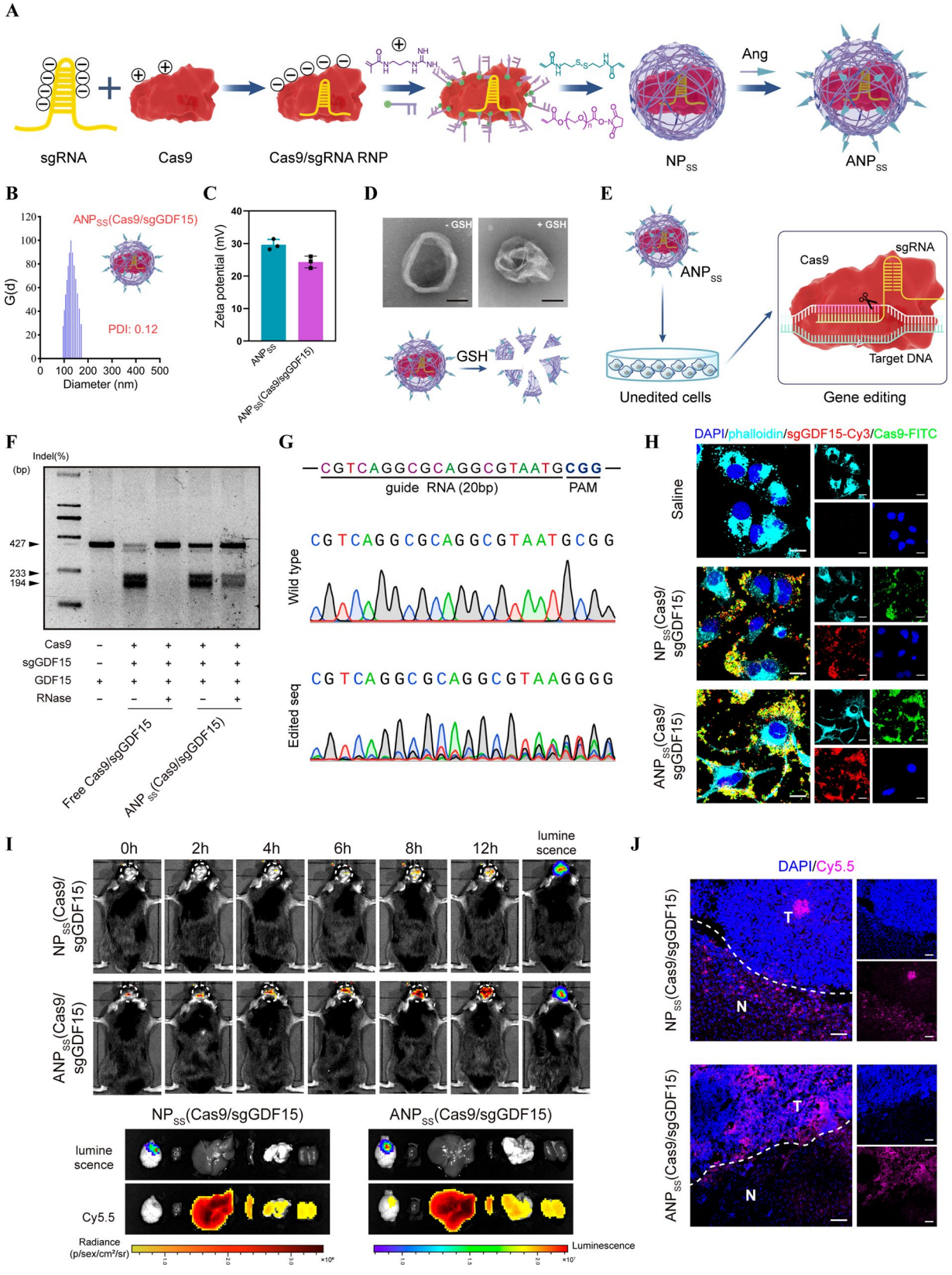

Fig. 3 (See legend on next page.)

(See figure on previous page.)

Fig. 3 Design and construction of ANP_{SS}(Cas9/sgGDF15). **(A)** Disulfide cross-linked nanoparticles containing Cas9/sgRNA were synthesized through in situ free-radical polymerization and functionalized with the Ang glioma-targeting peptide. **(B)** DLS image showing the particle size of ANP_{SS}(Cas9/sgGDF15). **(C)** Zeta potential of ANP_{SS}(Cas9/sgGDF15). **(D)** TEM images were taken to compare the spherical shape of the ANP_{SS}(Cas9/sgGDF15) in saline with or without GSH. **(E)** Schematic representation of genome editing by ANP_{SS}(Cas9/sgGDF15). **(F)** Agarose gel electrophoresis analysis was performed to observe insertions and deletions (indels) in the GDF15 gene following treatment with ANP_{SS}(Cas9/sgGDF15) or other specified treatments, with or without RNase treatment at a concentration of 2 mg/ml for 20 min. **(G)** GDF15 gene editing in GL261 cells treated with ANP_{SS}(Cas9/sgGDF15) was confirmed through DNA sequencing. **(H)** Immunofluorescence images showing NP_{SS}(Cas9/sgGDF15) and ANP_{SS}(Cas9/sgGDF15) uptake into GL261 cells. Scale bar, 10 μm **(I)** Fluorescence images of mice with orthotopic GL261 tumors were captured following the injection of NP_{SS}(Cas9/sgGDF15) or ANP_{SS}(Cas9/sgGDF15). **(J)** Confocal microscopy revealed the tumor penetration of NP_{SS}(Cas9/sgGDF15) and ANP_{SS}(Cas9/sgGDF15). Nuclei were counterstained with DAPI (blue), and Cy5.5-Cas9 fluorescence revealed a violet color. Dotted lines were used to outline the tumor boundary, with brain tissue labeled N and the tumor labeled T. Scale bar, 100 μm

constructed a spontaneous GBM model by using RCAS viruses carrying oncogenes to specifically infect tv-a-expressing cells on N/tv-a; Ink4a/$Arf^{-/-}$ mice [20]. Similar results were observed in the spontaneous GBM mouse model, indicating that ANP_{SS}(Cas9/sgGDF15) exhibited a higher targeting ability towards GBM compared to NP_{SS}(Cas9/sgGDF15) in vivo (Supplementary Fig. 12A-C). These results show that ANP_{SS} (Cas9/sgRNA) have excellent BBB penetration ability and successfully accumulate in tumors in a GL261-bearing mouse model and a spontaneous GBM mouse model.

Assessment of the effect of ANPSS(Cas9/sgGDF15) in the orthotopic GBM model

To evaluate the therapeutic potential of ANP_{SS}(Cas9/sgGDF15), the orthotopic GBM mouse models were established. The mice were randomly assigned to different treatment groups and received intravenous injections of saline, ANP_{SS}(Cas9/sgNC), or ANP_{SS}(Cas9/sgGDF15) every 7 days (Fig. 4A). Remarkably, mice treated with ANP_{SS}(Cas9/sgGDF15) exhibited a substantial decrease in tumor growth, as indicated by a noticeable reduction in bioluminescence signal intensity (Fig. 4B-C). Conversely, mice treated with saline or ANP_{SS}(Cas9/sgNC) presented an increase in bioluminescence signal intensity, indicating a lack of efficacy in suppressing tumor growth (Fig. 4D). Survival curve analysis demonstrated a significant improvement in median survival time, exceeding 41 days with ANP_{SS}(Cas9/sgGDF15) treatment compared to 31 and 32.5 days with saline and ANP_{SS}(Cas9/sgNC), respectively (Fig. 4E).

To confirm that the inhibition of tumor growth was attributed to the disruption of the GDF15 gene and the subsequent decrease in GDF15 protein expression, excised tumor tissues from mice treated with ANP_{SS}(Cas9/sgGDF15), ANP_{SS}(Cas9/sgNC), or saline were analyzed on day 28. The evaluation of gene editing efficiency, as indicated by the indel frequency, showed a notable 67.3% efficiency for ANP_{SS}(Cas9/sgGDF15) treatment (Fig. 4F). Furthermore, a significant reduction in GDF15 protein expression was noted in the group treated with ANP_{SS}(Cas9/sgGDF15) in comparison to the control group (Supplementary Fig. 13). Moreover, disruption of the GDF15 gene was verified through next-generation sequencing (NGS), which revealed a mutation rate of 59.4% (Fig. 4G). Immunohistochemical analysis showed a significant decrease in the presence of GDF15-positive tumor cells, and Ki67 and cleaved caspase-3 IHC staining confirmed the potent tumor inhibitory effect of ANP_{SS}(Cas9/sgGDF15) (Fig. 4H). Flow cytometry analysis demonstrated that the number of cytotoxic T lymphocytes ($CD3^+CD8^+GZMB^+$) was significantly greater in the ANP_{SS}(Cas9/sgGDF15) group than in the other treatment groups. Additionally, ANP_{SS}(Cas9/sgGDF15) treatment resulted in the lowest infiltration of M2-like TAMs ($CD86^-CD206^+$), with a greater number of M1-like TAMs ($CD86^+CD206^-$) within the tumors (Fig. 4I-K). Multiplex immunofluorescence analysis revealed a substantial increase in $CD3^+CD8^+GZMB^+$ T cells and M1-like TAMs after ANP_{SS}(Cas9/sgGDF15) treatment (Fig. 4L). These results indicate that targeting GDF15 with ANP_{SS}(Cas9/sgGDF15) in orthotopic GBM xenografts can remodel the TME and effectively suppress GBM progression.

In vivo antitumor activity of ANPSS(Cas9/sgGDF15) in the spontaneous GBM model

The above results indicate that ANP_{SS}(Cas9/sgGDF15) can exert significant antitumor effects in the orthotopic GBM models. To further confirm the antitumor effects of ANP_{SS}(Cas9/sgGDF15), we also conducted therapeutic evaluation experiments in the spontaneous GBM mouse model. We first analyzed GDF15 protein levels in glioma tissues and observed significantly higher GDF15 expression in the brains of spontaneous glioma model than in those of normal controls (Supplementary Fig. 14). The results were consistent with those observed in GL261-bearing mice, where ANP_{SS}(Cas9/sgGDF15) treatment successfully inhibited tumor growth, as evidenced by the reduction in tumor volume in treated mice (Fig. 5A-D). Additionally, mice treated with ANP_{SS}(Cas9/sgGDF15) showed a significant improvement in median survival (41 days), surpassing the median survival time (29 days) of mice treated with saline (Fig. 5E). T7E1 assays revealed a significant indel frequency of 61.3% in mice treated with ANP_{SS}(Cas9/sgGDF15) (Fig. 5F). Subsequent NGS

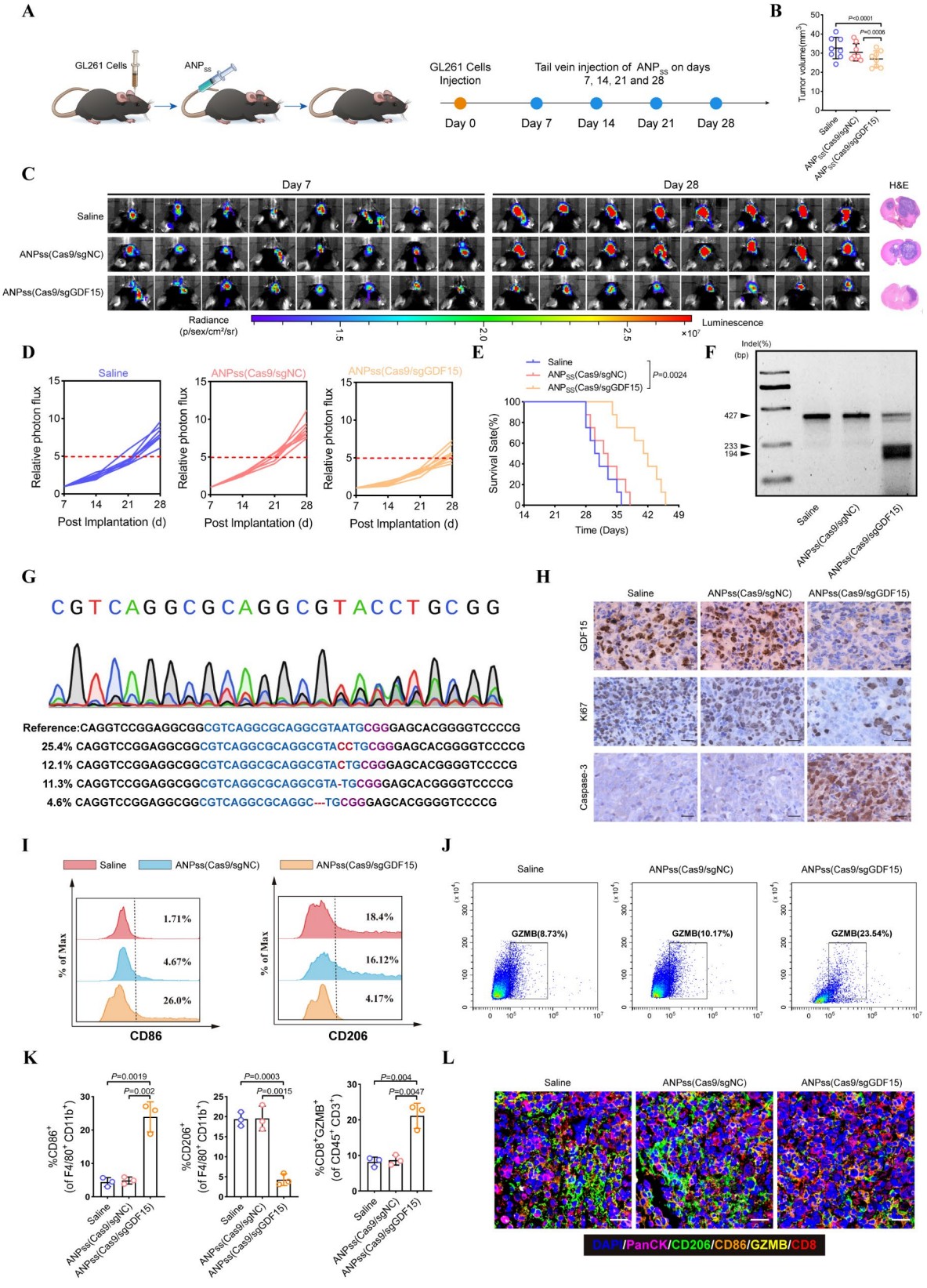

Fig. 4 (See legend on next page.)

(See figure on previous page.)

Fig. 4 Gene editing therapy of ANP_{SS}(Cas9/sgGDF15) in the GL261 orthotopic GBM mouse model. **(A)** Diagram illustrating the timeline of the study conducted using the GL261 orthotopic tumor model. The intravenous injection of normal saline, ANP_{SS} (Cas9/sgNC), or ANP_{SS}(Cas9/sgGDF15) (a 1.5 mg dose of Cas9 equivalent per kilogram) was performed on days 7, 14, 21, and 28 after tumor implantation. **(B)** Quantification of tumor volume in mice after the indicated treatments. **(C)** Images displaying luminescence in orthotopic GL261-bearing C57BL/6 mice following the indicated treatments. **(D)** Individual tumor growth curves of tumor-bearing mice subjected to various treatments. **(E)** Mouse survival after the indicated treatments was evaluated in another three groups of mice ($n = 8$). **(F)** Frequencies of indel mutations in the GDF15 gene observed in tumor tissues from mice subjected to various treatments. **(G)** The results of DNA sequencing showing GDF15 gene editing in GBM tumors excised from mice treated with ANP_{SS}(Cas9/sgGDF15). **(H)** Immunohistochemical analysis of GDF15, Caspase-3 and Ki67 expression in tumor tissues excised from mice subjected to the indicated treatments. Scale bar, 50 μm **I-K.** Flow cytometric quantification of $CD206^+$ TAMs, $CD86^+$ TAMs, and $CD3^+CD8^+GZMB^+$ T cells in tumors. **L.** Representative multiplex immunofluorescence staining of tumor tissues from mice treated with the indicated drugs on day 28 after tumor implantation. The stained markers included DAPI (blue), PanCK (pink), CD8 (red), GZMB (yellow), CD86 (orange), and CD206 (green). Scale bar, 50 μm

analysis confirmed efficient editing of the GDF15 gene, with an indel frequency of 56.8%, which was consistent with the T7E1 assay findings (Fig. 5G). Additionally, a reduction in GDF15 protein expression was noted in spontaneous glioma tissues, indicating a possible disruption of the GDF15 gene (Supplementary Fig. 15). Immunohistochemical analysis of cleaved caspase-3 and Ki67 signals in tumor tissues revealed a gradual increase in apoptosis in mice treated with ANP_{SS}(Cas9/sgGDF15), along with a subsequent decrease in cell proliferation (Fig. 5H). Furthermore, ANP_{SS}(Cas9/sgGDF15) therapy led to a decrease in the presence of $CD86^-CD206^+$ M2-like TAMs, while boosting the population of $CD86^+CD206$– M1-like TAMs in the tumor microenvironment (Fig. 5I). The tumors of the mice treated with ANP_{SS}(Cas9/sgGDF15) presented a significant increase in T-cell infiltration. Subsequent analysis revealed elevated levels of GZMB in $CD8^+$ T cells, suggesting increased cell lysis ability in the ANP_{SS}(Cas9/sgGDF15)-treated mice (Fig. 5J-K). Multiplex immunofluorescence examination also demonstrated a notable rise in $CD3^+CD8^+GZMB^+$ T cells and M1-like TAMs following ANP_{SS}(Cas9/sgGDF15) administration (Fig. 5L). These findings validated the immunostimulatory effects of ANP_{SS}(Cas9/sgGDF15) in mice with tumors, resulting in enhanced therapeutic outcomes in a spontaneous GBM model.

ANPSS(Cas9/sgGDF15) potentiates the efficacy of PD-1 blockade therapy

Immunotherapy with antibodies that target like PD-1 and CLTA-4 has shown different levels of effectiveness in the treatment of different types of cancers, such as hepatocellular carcinoma, melanoma and non-small cell lung cancer [21]. Nevertheless, research has suggested that the use of an α-PD-1 antibody does not result in improved overall survival rates in patients with GBM [22]. Crucially, the functional screening readouts in this study revealed that the sgRNAs targeting GDF15 were significantly depleted in the α-PD-1 group compared with the C57BL/6 group (Fig. 1E). This finding suggests that the loss of GDF15 may increase sensitivity to α-PD-1 therapy in GBM. To further investigate the efficacy of our constructed nanoparticles, GL261-bearing mice were randomly allocated to different groups and were subsequently administered intravenous tail vein injections of various substances, including saline, ANP_{SS}(Cas9/sgGDF15), α-PD-1, and a combination of ANP_{SS}(Cas9/sgGDF15) and α-PD-1 every 7 days. Notably, combination therapy demonstrated superior efficacy compared with the other treatments as evidenced by the intensity of the bioluminescence signal (Fig. 6A). In contrast, the mice that received saline presented increased bioluminescence intensity, indicating a faster rate of tumor growth. After the treatment period ended, the results revealed a notable reduction in tumor volume across all three intervention groups compared with the saline-treated group, among them, the combination therapy-treated group exhibited the smallest tumor volume (Fig. 6B). Survival curve analysis demonstrated that combination therapy significantly prolonged the median survival time to over 46 days and resulted in complete tumor eradication in 25% (2/8) of the mice. In contrast, the mice treated with saline exhibited a substantially shorter median survival time of 32 days (Fig. 6C). Moreover, NGS revealed that the gene editing efficiencies of ANP_{SS}(Cas9/sgGDF15) and the combination therapy were 55.9% and 57.4%, respectively (Fig. 6D). Furthermore, the examination of Ki67 and cleaved caspase-3 IHC staining evidenced the remarkable tumor inhibitory efficacy of ANP_{SS}(Cas9/sgGDF15) + α-PD-1 therapy (Fig. 6E). The synergistic effect of combining α-PD-1 with ANP_{SS}(Cas9/sgGDF15) led to an increased presence of M1-like TAMs and $GZMB^+CD8^+$ T cells in the TME (Fig. 6F-I). These findings suggest that inhibiting GDF15 genetically along with α-PD-1 therapy significantly hinders tumor growth, suggesting a promising therapeutic approach for immunologically 'cold' GBM.

ANPSS(Cas9/sgGDF15) exhibits a favorable safety profile

Owing to possible safety issues related to off-target effects, toxicity, and immunogenicity, a thorough evaluation is necessary for genome editing employing CRISPR/Cas9 technology. Initially, we examined the impact of ANP_{SS}(Cas9/sgGDF15) on the proliferation of diverse healthy cells, which encompass hepatic stellate cells LX-2,

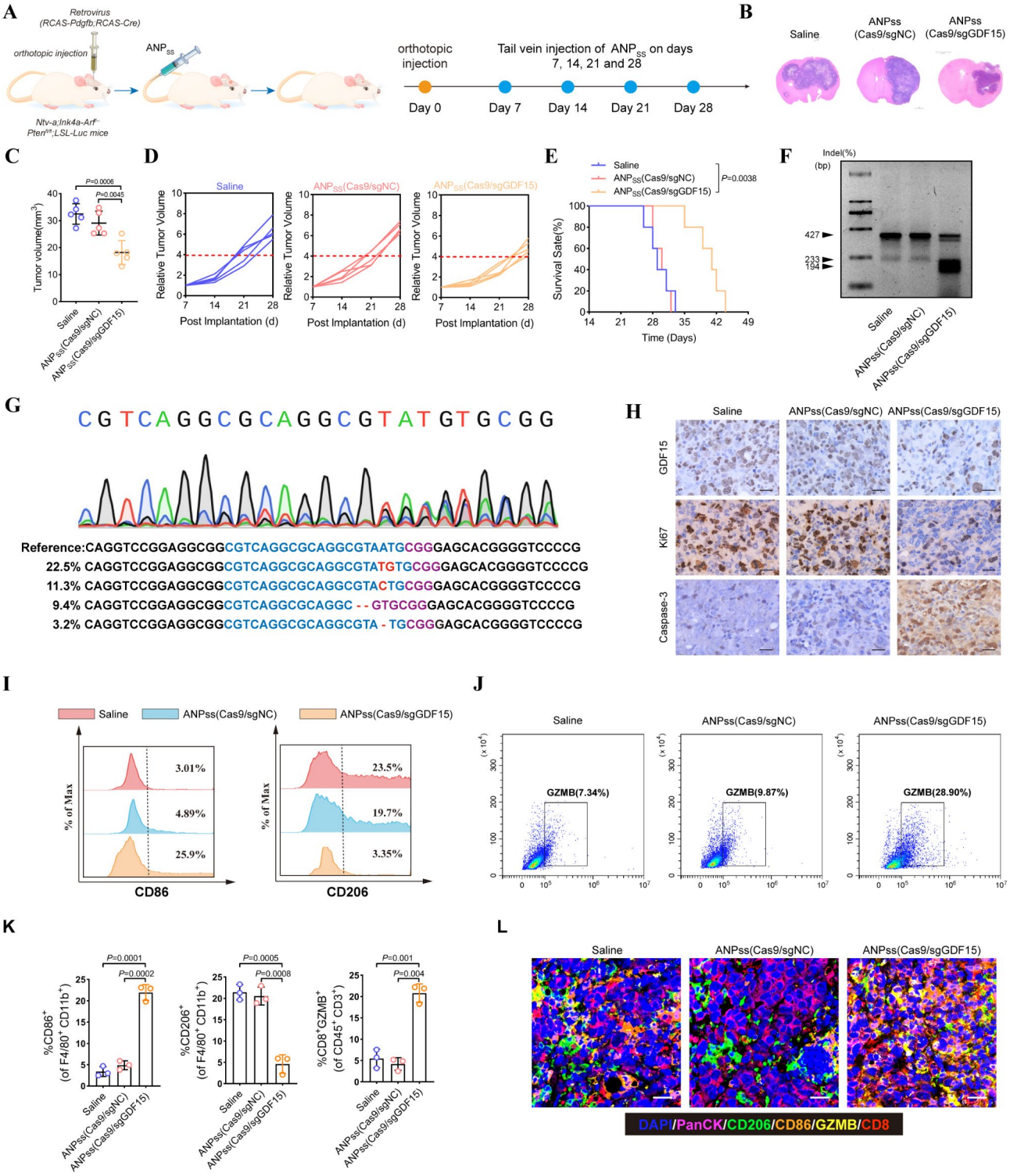

Fig. 5 Gene editing therapy of ANP_{SS}(Cas9/sgGDF15) in the spontaneous GBM mouse model. **A.** Schematic of spontaneous GBM model establishment. The intravenous injection of normal saline, ANP_{SS} (Cas9/sgNC), or ANP_{SS}(Cas9/sgGDF15) (a 1.5 mg dose of Cas9 equivalent per kilogram) was performed on days 7, 14, 21, and 28 after tumor implantation. **B**. H&E staining images of whole brains excised from mice treated as described above on day 20 and the tumor volume of each mouse. **C-D**. Individual tumor growth curves of tumor-bearing mice subjected to various treatments. **E.** Survival rates of the mice in the different groups ($n = 5$). **F.** Frequencies of indel mutations in the GDF15 gene observed in tumor tissues from mice subjected to the indicated treatments. **G.** Sequencing results of GDF15 gene editing in the spontaneous GBM model treated with ANP_{SS}(Cas9/sgGDF15) are presented. **H.** Immunohistochemistry analysis was conducted to assess the expression of GDF15, Caspase-3, and Ki67 in tumor tissues. Scale bar, 50 μm. **I-K.** Flow cytometric quantification of $CD206^+$ TAM, $CD86^+$ TAM, and $CD3^+CD8^+GZMB^+$ T cells in tumors. **L.** Multiplex immunofluorescence analysis of PanCK, CD8, GZMB, CD86, and CD206 expression

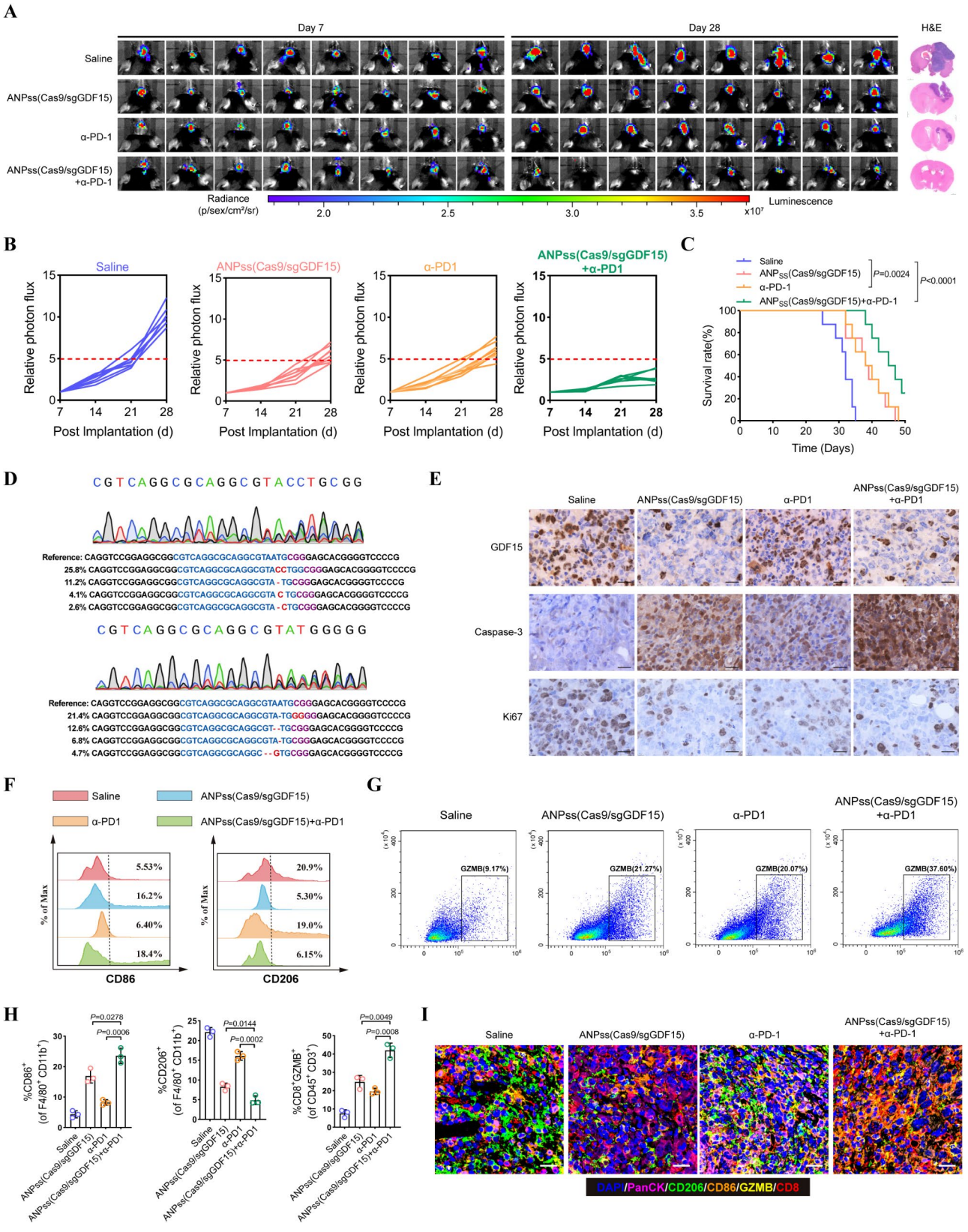

Fig. 6 (See legend on next page.)

(See figure on previous page.)

Fig. 6 Synergistic efficacy of ANP_{SS}(Cas9/sgGDF15) combined with an α-PD-1 antibody. **(A)** Fluorescence images of orthotopic GL261-bearing C57BL/6 mice following treatment with saline, ANP_{SS}(Cas9/sgGDF15), an α-PD-1 antibody, or ANP_{SS}(Cas9/sgGDF15) combined with the α-PD-1 antibody ($n = 8$). Tumor volumes of the different groups of mice at 20 days after implantation of GL261-Luc. **(B)** Individual GL261-Luc tumor growth curves of the mice after different treatments. **(C)** Kaplan–Meier survival curves of the mice that received different treatments. **(D)** The results of DNA sequencing revealed GDF15 gene editing in orthotopic GL261 tumors excised from mice treated with ANP_{SS}(Cas9/sgGDF15) in combination with α-PD-1 treatment. **(E)** Immunohistochemistry analysis was conducted to assess the expression of GDF15, Caspase-3, and Ki67 in tumor tissues. Scale bar,50 μm. **F-H.** Flow cytometric quantification of $CD206^+$ TAMs, $CD86^+$ TAMs, and $CD3^+CD8^+GZMB^+$ T cells in tumors. **I.** Multiplex immunofluorescence analysis of PanCK, CD8, GZMB, CD86, and CD206 expression. Scale bar, 50 μm

hepatocytes AML12, cardiomyocytes AC16, cardiac muscle cells HL-1, lung epithelial cells MLE12, and renal tubular cells TCMK-1. Notably, no significant alterations in the growth patterns of any of the cellular populations were detected (Supplementary Fig. 16). Afterward, a comprehensive examination of off-target effects was conducted by pinpointing the locations in the tumor tissue with the greatest potential for off-target changes in the genomic sequence, with a specific emphasis on GDF15. Following the administration of ANP_{SS}(Cas9/sgGDF15) to mice with GL261 tumors, NGS analysis indicated minimal gene disruption at the suspected locations within the tumor tissue. The mutation frequency was found to be less than 0.5% across all 5 hypothesized target sites in these models. Given the tendency of nanoparticles to accumulate in the brain, heart, liver, and kidneys, we further examined these organs to assess potential off-target effects. Interestingly, the mutation frequencies at the 5 potential off-target sites were also below 0.5% in the brain, heart, liver, and kidneys of mice bearing GL261 tumors (Supplementary Fig. 17A). Next, ANP_{SS}(Cas9/sgGDF15) was administered intravenously to healthy C57BL/6 mice on alternate days, a total of 4 times, in order to evaluate both the immune response and toxicity. Throughout the treatment period, biochemical profiles of the mice treated with ANP_{SS}(Cas9/sgGDF15) were virtually identical to those observed in the saline-treated group, suggesting that ANP_{SS}(Cas9/sgGDF15) exerted minimal to no negative effects on kidney and liver functions (Supplementary Fig. 17B-C). Moreover, cachexia caused by cancer is a common concern that associated with reduced quality of life and shortened lifespan. Elevated levels of GDF15 in the bloodstream is also related to cachexia and decreased survival rates in cancer patients [23]. We found that treatment with ANP_{SS}(Cas9/sgGDF15) prevents tumor-driven weight loss (Supplementary Fig. 18). These results suggest that the systemic delivery of ANP_{SS}(Cas9/sgGDF15) at therapeutic doses is safe and does not trigger an immune response. Nonetheless, a thorough evaluation of possible toxic effects is required for advancing to preclinical stages.

Discussion

The GBM TME dampens the immune response, reducing the efficacy of immune checkpoint blockade therapies [24]. Identifying novel targets to modulate the immunosuppressive TME in GBM is essential for enhancing the efficacy of immunotherapy. To identify potential immunotherapy targets involved in the complex interaction between the immune system and cancer cells, we developed a mouse sgRNA library that aligns with all known disease-related immune genes. Our customized in vivo CRISPR screen, which was based on disparities in the mouse immune system, was performed to identify changes in immune-related genes across various TMEs that are involved in immune surveillance and immune escape. These targets can be used to quickly develop new clinical treatments that benefit a considerable subset of patients with GBM. To our knowledge, this is the first reported screening that systematically identified immune modulators within the endogenous GBM immune microenvironment. We demonstrated that GDF15 is a crucial driver of immune escape and that genetic targeting of GDF15 sensitizes GBM to ICB therapy, leading to complete or partial regression and prolonged survival.

GDF15, also known as macrophage inhibitory cytokine-1, is a unique member of the transforming growth factor β superfamily [25]. It is distinguished by seven conserved cysteine residues that create a cysteine knot, which is a key feature of the TGF-β superfamily [26]. Correlations between GDF-15 and cancer progression have been reported in various types of cancer, such as gastrointestinal cancer, hepatocellular carcinoma, esophageal cancer, ovarian cancer, melanoma, and breast cancer [27–30]. The results of these studies suggest that GDF-15 is a promising marker for cancer development, progression and prognosis. We demonstrated that the tumor-suppressing effect of GDF15 KO in vivo most likely depended on the remodeling of the TME and disrupting GDF15 has the potential to reshape the immunosuppressive TME by promoting M1-like macrophage polarization and activating T cells. Moreover, the expression level of GDF15 is significantly lower in healthy tissues than in cancerous tissues. Importantly, $GDF15^{-/-}$ mice presented no apparent disease characteristics, confirming the safety of GDF15 inhibition therapies [31]. Several pharmaceutical companies have initiated studies on GDF15 monoclonal antibodies to treat malignant tumors and cachexia induced by advanced cancer [32, 33]. However, the long-term use of monoclonal antibodies poses challenges due to off-target effects and the formation of anti-drug antibodies.

To enhance the inhibition of GDF15, we employed gene editing techniques to deactivate GDF15 in tumor cells at the genetic level. This approach offers improved targeting, specificity, and long-term effectiveness, presenting a new strategy for GDF15-targeted immunotherapy in GBM. Current methods for delivering CRISPR-Cas9 to brain include the use of viral vectors and nonviral synthetic delivery systems. Although these approaches have shown promising results in live organisms, they also have limitations that need to be addressed before potential human clinical applications can be considered. Viral vector delivery can trigger immune responses and off-target effects, presenting challenges for large-scale production [34]. Moreover, current nonviral delivery systems have drawbacks, including low loading efficiency, nonspecific targeting, issues with clearance from the brain, a risk of neuroinflammation, and the absence of responsive drug release mechanisms [35]. These systems also struggle with limited penetration of the BBB and cannot target specific brain disease sites. To address these challenges, a nonviral CRISPR–Cas9 delivery system was developed. This system uses angiopep-2-functionalized biodegradable nanoparticles, ANP_{SS}(Cas9/sgRNA), to encapsulate and protect the Cas9 protein and sgRNA, facilitating precise gene editing. ANP_{SS}(Cas9/sgGDF15) were designed to encapsulate a single Cas9 ribonucleoprotein/sgRNA with a loading efficiency close to 100%. Moreover, an important design feature includes the incorporation of disulfide bonds (-SS-) within the nanoparticles. These bonds serve two essential functions: protecting the Cas9/sgRNA complex from enzymatic degradation in the bloodstream and facilitating rapid release of Cas9/sgRNA in response to the intracellular reducing environment. The high levels of GSH present in tumor cells can break disulfide bonds, resulting in degradation of the nanoparticles. Another important design aspect was the modification of the outer shell of Cas9/sgRNA nanoparticles with the angiopep-2 peptide. This peptide specifically binds to the receptor LRP-1, which is highly expressed on both the endothelial cells of the BBB and GBM cells.

In conclusion, we conducted an in vivo CRISPR screen and discovered that GDF15 plays a crucial role in immune evasion and is a promising target for enhancing GBM immunotherapy. Genetic depletion of GDF15 through a noninvasive GBM delivery system can remodel the TME and ameliorate the immunosuppressive microenvironment. Our study presents a technique for incorporating CRISPR library screen with CRISPR-Cas9 gene therapy for the treatment of GBM and various tumors.

Materials and methods

Cell Culture

Mouse GBM cell line GL261, LX-2, AML12, AC16, HL-1, MLE-12 and DF-1 cells were obtained from ATCC and cultured in DMEM (Gibco, USA) containing 10% FBS and 1% penicillin/streptomycin (NCM, Suzhou, China).

CRISPR-Cas9 screen and data analysis

The lentiviral murine CRISPR-Cas9 knockout (MusCK) library consists of 49,252 guide RNAs targeting 4,922 mouse genes associated with immune modulation, along with 1000 control gRNAs in each half-library. GL261 cells were transduced with the Mouse CRISPR Knockout library using lentivirus at a multiplicity of infection of 0.3. Our results demonstrated a high coverage of the sgRNA library, with less than 0.25% missing sgRNAs observed across samples. The procedure for analyzing the sgRNA library consisted of a two-step PCR process. In the first PCR step, an ample amount of genomic DNA was utilized to ensure the preservation of the entire library complexity. Subsequently, in the second PCR step, the addition of specific sequencing adapters was performed on the products obtained from the initial PCR amplification.

Histology and immunohistochemistry

Samples of tissues were fixed in 4% paraformaldehyde for 48 h. Subsequently, the tissues were subjected to a series of procedures such as washing in PBS, dehydration in ethanol, and embedding in paraffin following transfer to xylene. The paraffin-embedded tissues were then sliced into 4 μm sections for H&E staining and immunohistochemical staining.

Orthotopic glioblastoma mouse model

To establish the orthotopic Glioblastoma model, luciferase-expressing GL261 cells were intracranially administered to Male C57BL/6 mice (6–8 weeks old) using a precise small animal stereotactic device. The injection site was targeted to the right side of the sagittal suture at a depth of 2.5 mm, with the focal point at 0.5 mm. A dental drill with a 0.7 mm diameter was used to create openings at the specified location. After successful tumor engraftment, D-Luciferin potassium salt was administered intraperitoneally given to visualize and document changes in intracranial tumor volume with a compact animal fluorescence imager.

Spontaneous glioblastoma mouse model

N/tv-a; $Ink4a/Arf^{-/-}$ mice were injected with DF-1 cells producing RCAS viruses in 6–7 weeks old according to the described protocol. The coordinates were: 0.5 mm anterior of bregma,1.2 mm lateral, and 2.5 mm ventral. Mice were monitored daily for signs of brain tumors and euthanized via CO_2 either upon detection of symptoms or at 12 weeks post-injection if no symptoms were present. The brains of euthanized mice were fixed in 4% paraformaldehyde for a minimum of 24 h and then embedded in paraffin for histological examination.

Western blot

Protein samples underwent resolution by SDS–PAGE and transfer to polyvinylidene difluoride membranes (Millipore, USA). The incubation of the primary antibodies (GDF15, Santa, sc-377195) was performed overnight at a temperature of 4 °C. Following this step, the signals were detected using secondary antibodies conjugated with peroxidase and captured using the Tanon5200 system.

Flow cytometry analysis

The tumors were trypsinized, then washed in PBS containing 2% FBS, and finally incubated with antibodies targeting cell surface proteins according to the instructions. The samples were then analyzed using a Becman-Coutler flow cytometry system.

Analysis of RNase Protection Assay

A combination of free Cas9/sgGDF15 and ANP_{SS}(Cas9/sgGDF15) was incubated with a solution containing RNase A at 37 °C for 30 min. Following this, the targeted DNA was introduced and allowed to incubate at for 60 min to evaluate its ability to induce DNA double-strand breaks in the target DNA. After this, the specified DNA was inserted and permitted to incubate at 37 °C for 60 min to assess its capacity to cause DNA double strand breaks in the designated DNA.

Immunofluorescence

The process of immunofluorescence staining and imaging adhered to standard procedures. In the case of GBM tumors, PBS-washed 8-μm frozen sections underwent blocking using a 5% goat serum blocking buffer in PBS at room temperature for 1 h. Primary antibodies were applied to the sections overnight at 4 °C, after which PBS was used for post-washing. Next, secondary antibodies were added to the slides and incubated for 1 h at room temperature.

T7E1 assays and Sanger sequencing

The T7E1 assay was used to assess the efficacy of editing targeted genomic loci. Cells or tissue samples were collected and DNA was extracted using DNA Isolation Kit from Ribobio. PCR amplification of each specific genomic locus was carried out using the FastPure Gel DNA Extraction Mini Kit. Subsequently, the standard T7E1 assay was conducted. The disrupted segments on the gel were visualized using a gel documentation system and analyzed with ImageJ software.

Enzyme-linked immunosorbent assay

C57BL/6 mice were transplanted with GL261 cells containing either vector control or sgGDF15. ELISA assays with a GDF15 antibody were then performed following the manufacturer's protocol.

Transmission electron microscopy

An aqueous solution containing ANP_{SS}(Cas9/sgGDF15) was dried on a carbon-coated copper grid and subsequently examined using a JEOL 1200 EX transmission electron microscope.

Mass cytometry (CyTOF)

Mass cytometry and data analysis were conducted by Puluoting Health Tech Co., Ltd. (HangZhou, China). Briefly, cells underwent filtration using a 70-μm cell strainer followed by incubation with an anti-mouse CD16/32 mAb for 10 min at room temperature to block Fc receptors. Afterward, 3×10^6 cells per sample were stained with a combination of metal-labeled mAbs targeting cell surface markers, processed with Fixation/Permeabilization Buffer, and then incubated with various mAbs against intracellular proteins. Following that, 1×10^6 cells per sample were diluted in ddH_2O with beads and evaluated using a mass cytometer (CyTOF, Fluidigm).

Synthesis of ANPSS(Cas9/sgGDF15)

Synthesis Process: Mix Cas9 (16.5 μg) and sgGDF15 (4.0 μg) at a molar ratio of 1:1.2 in 500 μL of HEPES buffer (10 mM, pH 7.4) and incubate at room temperature for 5 min. Subsequently, add 44 μg of acrylate PEG glycol succinimidyl carboxymethyl ester (ACLT-PEG-SCM) and stir for 10 min. Following this, add 5 μg of acrylate guanidine solution (1 mg/mL) and allow the mixture to react for 5 min.The reaction is then continued with the addition of the degradable crosslinker N, N'-bis(acryloyl) cystamine. Polymerization is initiated by adding 3 μL of the catalyst ammonium persulfate (1 mg/mL) along with an equal volume of 1% (v/v) initiator N, N,N',N'-tetramethylethylenediamine. After reacting at 4 °C for 90 min, Angiopep-2 (154 μg) is introduced and conjugated to the surface of the nanoparticle via amide bond formation with the PEG termini. Purification: The reaction mixture is ultrafiltrated and washed with PBS (10 mM, pH 7.4) solution to remove unreacted free peptides, monomers, cross-linkers and initiators to obtain the final nanoparticle ANP_{SS} (Cas9/sgGDF15).

Safety evaluation

Male C57BL/6 mice, aged ten weeks, were intravenously injected with ANP_{SS}(Cas9/sgGDF15). Blood samples were collected for biochemistry analysis twenty-four hours post-injection. Biochemistry analysis was performed using the Cobas-6000 instrument, while complete blood count was conducted using the Sysmex.

Statistical analysis

Statistical analysis was performed with GraphPad Prism 8. Descriptions of the specific statistical tests can be found in the captions of the figures. The data is presented as mean values along with their corresponding standard deviations. Statistical significance was represented as: * for $P < 0.05$, ** for $P < 0.01$, and *** for $P < 0.001$.

Supplementary Information

The online version contains supplementary material available at https://doi.org/10.1186/s12951-025-03182-8 .

Supplementary Material 1

Acknowledgements

We would like to thank all the creators and curators of the publicly available datasets used in this study and the developers of the open-source software packages.

Author contributions

C.Z., X.L. and W.Z.W. carried a majority of experiments and analyzed data. J.T.G. and M.L. wrote the main manuscript. C.Z., X.L. and W.L. prepared figures. L.H. and A.A.Y. engineered and constructed the Nanoparticles. Z.C.C., M.R.Z. and Y.X.W. provided support for animal experiment. W.L.L., J.Y.M., Y.L.H. and Y.Q.Z. analyzed the bioinformatic data. S.N.W., W.Q.Z.and W.Liu. performed the statistical analysis. K.Z., J.T.G. and M.L. conceived the study, designed the study, evaluated data and revised the manuscript.

Funding

This work was supported by the National Natural Science Foundation of China (82003220); National Defense Biotechnology Fund for Outstanding Young Talents 01-SWKJYCJJ17; The Natural Science Basic Research Program of Shaanxi Province (2022JM-51); Natural Science Foundation of Shaanxi(2020JQ-445).

Data availability

No datasets were generated or analysed during the current study.

Declarations

Ethics approval and consent to participate

The project was approved by the Institutional Animal Care and Use Committee at the Air Force Medical University(IACUC-20220907).

Consent for publication

All authors have agreed to publish this manuscript.

Competing interests

The authors declare no competing interests.

Author details

[1]State Key Laboratory of Cancer Biology, Biotechnology Center, School of Pharmacy, The Fourth Military Medical University, Xi'an, China
[2]Department of Neurosurgery, Xijing Hospital, Xi'an, China
[3]Department of Plastic and Reconstructive Surgery, Xijing Hospital, Fourth Military Medical University, Xi'an, China
[4]Shaanxi Provincial Key Laboratory of Clinic Genetics, Fourth Military Medical University, Xi'an, China
[5]Department of Aviation Medicine, Xijing Hospital, Xi'an, China

Received: 14 October 2024 / Accepted: 1 February 2025
Published online: 20 February 2025

References

1. Saratsis A M, Knowles T, Petrovic A, et al. H3K27M mutant glioma: Disease definition and biological underpinnings[J]. Neuro Oncol. 2024;26(Supplement2):S92–100.
2. Turco V, Pfleiderer K, Hunger J, et al. T cell-independent eradication of experimental glioma by intravenous TLR7/8-agonist-loaded nanoparticles[J]. Nat Commun. 2023;14(1):771.
3. Jiang L, Hao Y, Shao C et al. ADAR1-mediated RNA editing links ganglioside catabolism to glioblastoma stem cell maintenance[J]. J Clin Invest, 2022, 132(6).
4. Wang F, Zhao F, Zhang L, et al. CDC6 is a prognostic biomarker and correlated with immune infiltrates in glioma[J]. Mol Cancer. 2022;21(1):153.
5. Kong J, Zou R, Law GL, et al. Biomimetic multifunctional persistent luminescence nanoprobes for long-term near-infrared imaging and therapy of cerebral and cerebellar gliomas[J]. Sci Adv. 2022;8(10):eabm7077.
6. Greten T F, Villanueva A, Korangy F, et al. Biomarkers for immunotherapy of hepatocellular carcinoma[J]. Nat Rev Clin Oncol. 2023;20(11):780–98.
7. Morad G, Helmink B A, Sharma P, et al. Hallmarks of response, resistance, and toxicity to immune checkpoint blockade[J]. Cell. 2021;184(21):5309–37.
8. Mitra A, Kumar A, Amdare N P et al. Current Landscape of Cancer Immunotherapy: harnessing the Immune Arsenal to Overcome Immune Evasion[J]. Biology, 2024, 13(5).
9. Agosti E, Zeppieri M, De Maria L et al. Glioblastoma Immunotherapy: a systematic review of the Present strategies and prospects for Advancements[J]. Int J Mol Sci, 2023, 24(20).
10. Yuan B, Wang G, Tang X, et al. Immunotherapy of glioblastoma: recent advances and future prospects[J]. Hum Vaccin Immunother. 2022;18(5):2055417.
11. Leuzzi G, Vasciaveo A, Taglialatela A, et al. SMARCAL1 is a dual regulator of innate immune signaling and PD-L1 expression that promotes tumor immune evasion[J]. Cell. 2024;187(4):861–e881832.
12. Chen X, Lu Q, Zhou H, et al. A membrane-associated MHC-I inhibitory axis for cancer immune evasion[J]. Cell. 2023;186(18):3903–20. e3921.
13. Griffin G K, Wu J, Iracheta-vellve A, et al. Epigenetic silencing by SETDB1 suppresses tumour intrinsic immunogenicity[J]. Nature. 2021;595(7866):309–14.
14. Pan D, Kobayashi A, Jiang P, et al. A major chromatin regulator determines resistance of tumor cells to T cell-mediated killing[J]. Science. 2018;359(6377):770–5.
15. Wang X, Tokheim C, Gu S S, et al. In vivo CRISPR screens identify the E3 ligase Cop1 as a modulator of macrophage infiltration and cancer immunotherapy target[J]. Cell. 2021;184(21):5357–e53745322.
16. Manguso R T, Pope H W, Zimmer M D, et al. In vivo CRISPR screening identifies Ptpn2 as a cancer immunotherapy target[J]. Nature. 2017;547(7664):413–8.
17. Paul S, Chhatar S, Mishra A, et al. Natural killer T cell activation increases iNOS(+)CD206(-) M1 macrophage and controls the growth of solid tumor[J]. J Immunother Cancer. 2019;7(1):208.
18. Tammam S N, Azzazy H M E Lamprechta. Nuclear and cytoplasmic delivery of lactoferrin in glioma using chitosan nanoparticles: Cellular location dependent-action of lactoferrin[J]. Eur J Pharm Biopharm. 2018;129:74–9.
19. Di Polidoro A C, Cafarchio A, Vecchione D et al. Revealing Angiopep-2/LRP1 Molecular Interaction for Optimal Delivery to Glioblastoma (GBM)[J]. Molecules, 2022, 27(19).
20. Uhrbom L, Kastemar M, Johansson F K, et al. Cell type-specific tumor suppression by Ink4a and Arf in Kras-induced mouse gliomagenesis[J]. Cancer Res. 2005;65(6):2065–9.
21. Ramos-casals M, Brahmer J R, Callahan M K et al. Immune-related adverse events of checkpoint inhibitors[J]. Nat Reviews Disease Primers, 2020, 6(1).
22. Yu MW, Quail DF. Immunotherapy for glioblastoma: current progress and challenges. Front Immunol. 2021;12:676301.
23. Suriben R, Chen M, Higbee J, et al. Antibody-mediated inhibition of GDF15-GFRAL activity reverses cancer cachexia in mice[J]. Nat Med. 2020;26(8):1264–70.
24. Lin H, Liu C. Understanding the immunosuppressive microenvironment of glioma: mechanistic insights and clinical perspectives[J]. J Hematol Oncol. 2024;17(1):31.
25. Wang Z, He L, Li W et al. GDF15 induces immunosuppression via CD48 on regulatory T cells in hepatocellular carcinoma[J]. J Immunother Cancer, 2021, 9(9).
26. Rochette L, Zeller M, Cottin Y, et al. GDF15: an emerging modulator of immunity and a strategy in COVID-19 in association with iron metabolism[J]. Trends Endocrinol Metab. 2021;32(11):875–89.

27. Myojin Y, Hikita H, Sugiyama M, et al. Hepatic stellate cells in Hepatocellular Carcinoma promote Tumor Growth Via Growth differentiation factor 15 Production[J]. Gastroenterology. 2021;160(5):1741–e17541716.
28. Baek SJ, Eling T. Growth differentiation factor 15 (GDF15): a survival protein with therapeutic potential in metabolic diseases[J]. Pharmacol Ther. 2019;198:46–58.
29. Tanno T, Lim Y, Wang Q, et al. Growth differentiating factor 15 enhances the tumor-initiating and self-renewal potential of multiple myeloma cells[J]. Blood. 2014;123(5):725–33.
30. Ratnam N M, Peterson J M, Talbert E E, et al. NF-kappaB regulates GDF-15 to suppress macrophage surveillance during early tumor development[J]. J Clin Invest. 2017;127(10):3796–809.
31. Wang D, Day E A, Townsend L K, et al. GDF15: emerging biology and therapeutic applications for obesity and cardiometabolic disease[J]. Nat Rev Endocrinol. 2021;17(10):592–607.
32. Groarke JD, Crawford J, Collins S M, et al. Phase 2 study of the efficacy and safety of ponsegromab in patients with cancer cachexia: PROACC-1 study design[J]. J Cachexia Sarcopenia Muscle. 2024;15(3):1054–61.
33. Albuquerque B, Chen X, Hirenallur-shanthappa D et al. Neutralization of GDF15 prevents Anorexia and Weight loss in the Monocrotaline-Induced Cardiac Cachexia Rat Model[J]. Cells, 2022, 11(7).
34. Wang J-H, Gessler D J, Zhan W, et al. Adeno-associated virus as a delivery vector for gene therapy of human diseases[J]. Volume 9. Signal Transduction and Targeted Therapy; 2024. 1.
35. Taghdiri M. Mussolino C. Viral and non-viral systems to deliver gene therapeutics to clinical Targets[J]. Int J Mol Sci, 2024, 25(13).

Publisher's note